SEMARAK ILMU PUBLISHING

Semarak Engineering Journal

Journal homepage:
https://semarakilmu.my/index.php/sej/index
ISSN: 3036-0145

Trenched No-core Fiber based Refractive Index Sensor

Tan Jin Wen[1], Fauzan Ahmad[1,*]

[1] Advance Vehicle System (AVS), Electronic System Engineering, Malaysia-Japan International Institute of Technology, Universiti Teknologi Malaysia, Jalan Sultan Yahya Petra, Kampung Datuk Keramat, 54100 Kuala Lumpur, Malaysia

ARTICLE INFO

Article history:
Received 7 September
Received in revised form 5 October 2023
Accepted 1 December 2023
Available online 28 December 2023

Keywords:
No-core fiber; COMSOL; sensor

ABSTRACT

Refractive-index (RI) measurement of a substance is widely used in many applications such as monitoring environmental pollution, measuring the concentration of substances and determining the composition of the solution. The objective of this study is to evaluate the sensitivity of RI measurement using trenched no core fiber (trench-NCF) with different RI analyte ranges from 1.31-1.448. This work proposed a simulation of trench no core fiber sensor for evanescent study in exposing the trench-NCF in different RI analytes using COMSOL Multiphysics software. The fabrication process is implemented by splicing the two ends of the trench-NCF with two single-mode no-core fiber. Then, one end is connected to the amplified spontaneous emission (ASE) broadband source while the other end is connected to the optical spectrum analyzer (OSA) while testing different RI analyte. Data was retrieved from the OSA showing the dip wavelength increases in a non-linear pattern when RI increases. Linear fitting was applied to obtain the sensitivity of 148.06nm/RIU and 1626.1nm/RIU in the range of 1.310 RIU to 1.421 RIU and 1.412 to 1.448 RIU respectively. In the future, the results and simulations can be used as a reference in future study in implementing a fiber-optic based refractive-index sensor.

1. Introduction

In recent years, fiber optic sensors have successfully replaced many traditional sensors for measurements such as temperature, strain, chemical substances and magnetic field measurement [1,4,14,15]. Optical fiber is a dielectric medium and the optical transducer device used is also made with a dielectric material which is why they are chemically inert and immune to electromagnetic interference [5,6]. Putting aside their working principles and purposes of serving as a measurement sensor, fiber optics sensors comprise of the same set of components i.e., light sources, photodetectors, and optical components in guiding the light in between [7]. The fiber will transmit the optical field to the measurement region without the need for wiring the power source to the sensor compared to the conventional sensors. In this research, a thinner trenched no-core fiber (trench-NCF) is used as it exhibits a more sensitive response to environmental changes [2,13]. The primary refractive index (RI) sensing mechanism of using an NCF sensor is based on the wavelength

* *Corresponding author.*
E-mail address: fauzan.kl@utm.my

https:/doi.org/10.27934/sej.3.1.18b

shift of multimode signals' interference (MMI) [8-10]. To determine the sensitivity of the sensor, a particular length of the trench-NCF is used to be fabricated with multimode fiber and the light source is connected as input [11,12]. Different RI analyte is used to test the sensor by obtaining the wave spectrum using an Optical Spectrum Analyzer (OSA). The process of setting up the sensor is normally inexpensive and is not complicated.

2. Methodology

2.1 Simulation Procedure

Simulation is carried out to show the sensor behavior in different analyte RI using COMSOL Multiphysics software. A few steps have been taken accordingly in using the software to show the dedicated sensor model that can be represented interactively and virtually using the software. A better understanding of the trench-NCF in different RI analytes will be presented through simulated graphs and diagrams and can be compared with the result analyzed physically through fabrication. The simulation starts with geometry modelling. The geometry of the desired sensor design and specification is drawn. The drawn geometry inside the COMSOL GUI is called domain as shown in Figure 1. Then, the domain will be assigned to its respective RI and material. Next, the domain will be meshed for finite element analysis (FEA), a mathematical technique by discretizing them into small elements. Lastly, the result of the simulation is computed by running the simulation.

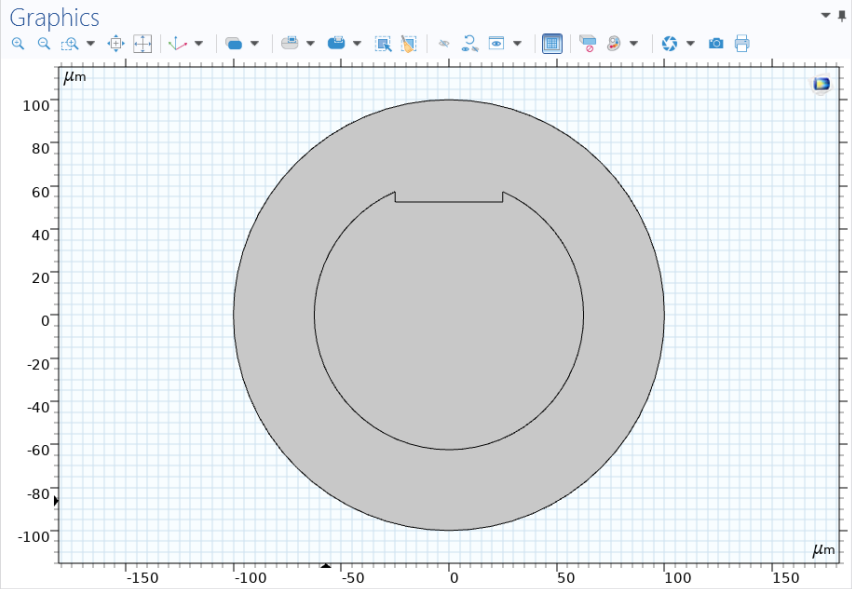

Fig. 1. Domain of trench-NCF in COMSOL GUI

2.2 Fabrication Procedure

First, the SMF (SMF-28e, Corning) and trench-NCF were cut to 30 cm and 3 cm, respectively by using fiber stripper (SS03, Fujikura) and the length was measured using the commercial ruler. 2 cm length of buffer coating was carefully stripped using fiber stripper. Then, cleaved to 1 cm using fiber cleaver (FC-6S, Sumitomo Electric), leaving the 1 cm length. Before splicing, the fiber was cleaned using isopropyl alcohol and gently wiped using clean wipes (Kimberly-Clark, KimwipesTM) to remove excess buffer coating and avoid any issues during splicing. The SMF and trench-NCF were spliced together using arc fusion splices (SignalFire, AI-7) as shown in Figure 2.

Fig. 2. Optical fiber fusion splicer

2.3 Characterization Procedure for Trench-NCF

The characterization procedure of the experiment is illustrated in Figure 3(a) and the real experiment is shown in Figure 3(b). The experiment is performed by selecting an appropriate wavelength of 1450nm to 1650nm of the ASE operating wavelength and 13dBm maximum power output. For the sensing system, an optical spectrum analyzer (OSA) (Yokogawa, AQ6370D) is used to record and monitor the changes in the spectrum.

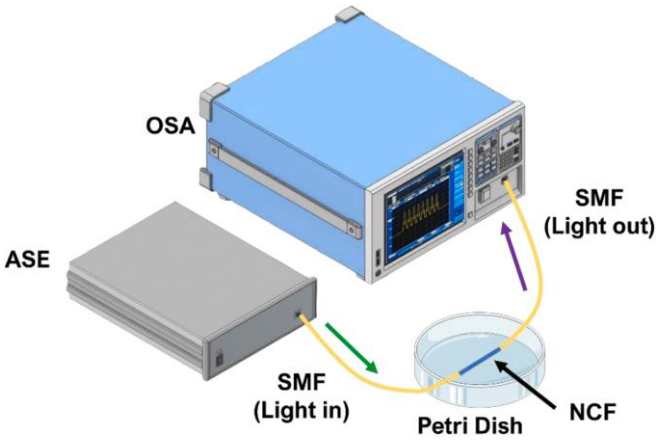

(a)

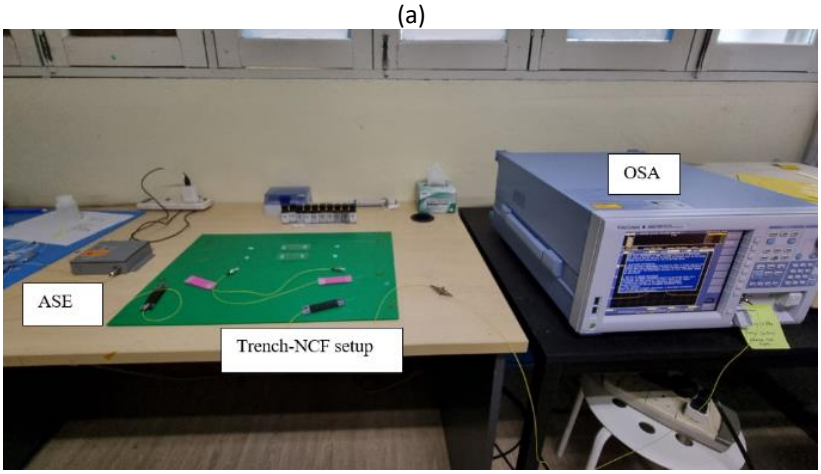

(b)

Fig. 3. Experimental setup for trench-NCF RI sensor (a) Illustration and (b) Real experiment setup

The trench-NCF is placed onto a petri dish as shown in Figure 4 and the fiber is made straight to reduce the environmental disturbances that might affect the accuracy of the measuring process. The power reading of the sensors with the ASE source is measured to make sure that the value does not exceed the stated value from OSA, 10 dBm. Analytes RI used which are 1.31, 1.33, 1.35, 1.37, 1.39, 1.412, 1.432, 1.44, 1.444 and 1.448. The measurement is carried out with the wavelength range of 1400 nm-1700 nm and 0.5 nm resolution. The first reading is recorded by connecting the ASE source to the OSA without the trench-NCF sensor to measure the wave spectrum of the source. The measurement is recorded and saved inside a USB flash drive. Then the trench-NCF is connected to the ASE source and OSA to measure the air spectrum and different analyte RI. The spectrum is recorded, saved into a USB flash drive, and repeated 5 times to be analyzed for further study.

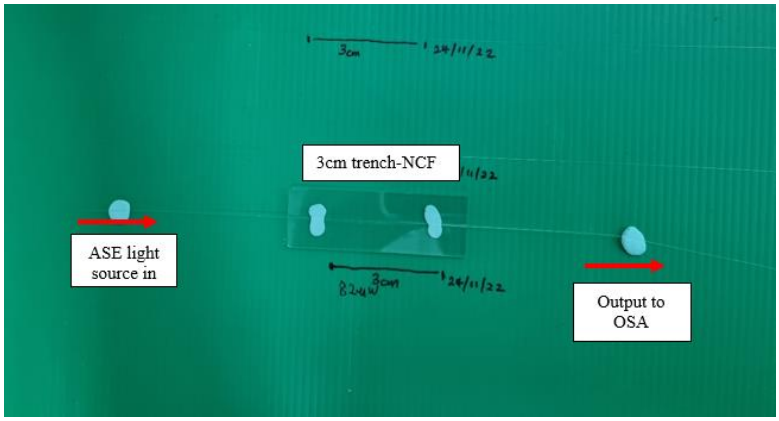

Fig. 4. Trench-NCF fixed on a glass slide

3. Result

3.1 Simulation Result

Figure 5 shows the simulated trench-NCF sensor results of electric field distribution in an air medium with an RI of 1.000 RIU obtained from the cross-section method. The red and blue colours represent the maximum and minimum electric field intensity respectively. From Figure 5, the coloured region shows the cross-sectional view of the trench-NCF sensor in the first linearly polarized (LP_{01}) mode profile. The fact that the electric field is evenly distributed and concentrated in the center suggests that the light is contained within the fiber. The faded region of the trench-NCF shows that the electric field is gradually decreasing when reaching the boundary between trench-NCF and analyte. This is due to the light energy attenuation as it reaches the boundary with different RI mediums. The mode field diameter graph (MFD) is plotted as shown in Figure 6(a). The evanescent wave from Figure 5 is difficult to see when changing the analyte RI in the COMSOL software because it is too small compared to the domain dimension. Therefore, a graph of MFD in Figure 6(b) is plotted to show the evanescent wave of the trench-NCF simulated in different RI. From Figure 6(b), the evanescent wave shifted to the right of the graph when the RI increased from 1.0 (air) to 1.4379 (analyte).

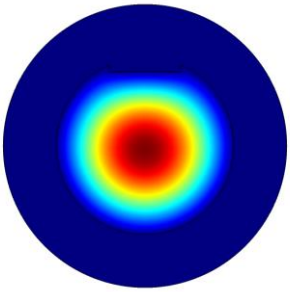

Fig. 5. Cross-sectional view of trench-NCF showing electric field intensity in air

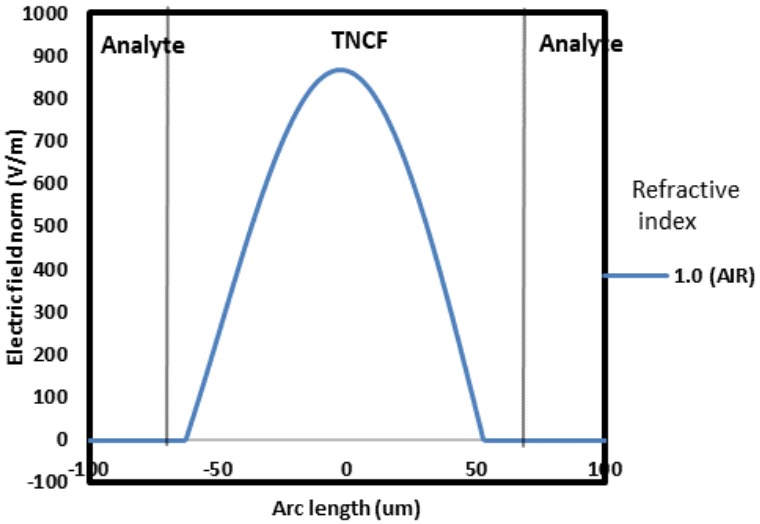

(a)

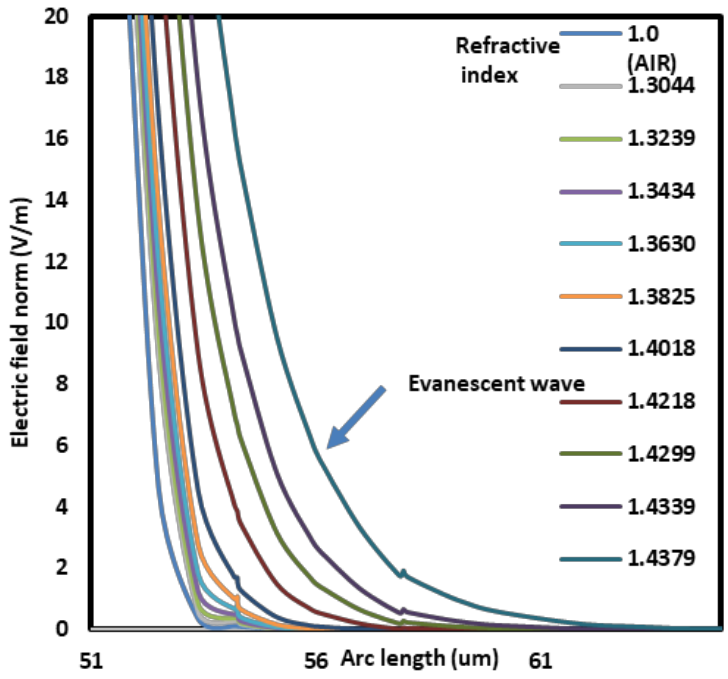

(b)

Fig. 6. Mode field graph of trench-NCF (a) in air and (b) showing the evanescent wave

3.2 Characterization Results and Discussion

The ASE source spectrum is measured using OSA. From the spectrum, the peak wavelength equal to 1531.21nm is defined as the sensor's operating wavelength. The spectrum loss P_L is calculated using Eq. (1)

$$\mathrm{P_L}(\lambda) = \mathrm{P_{out}} - \mathrm{P_{in}} \quad (1)$$

where P_L is the transmission loss spectrum in decibel (dB) unit, P_{out} represent the received or collected spectrum and P_{in} represent the ASE spectrum launched to the sensing system. P_{in} and P_{out} are computed from the OSA defined in decibels per milliwatts (dBm) unit. From Figure 7(a) the dip wavelength can be seen which can be used to determine the RI measurement of a liquid. The same analysis is carried out to obtain the transmission loss spectrum for all the different RI analytes and the dip wavelength is obtained as shown in Figure 7(b).

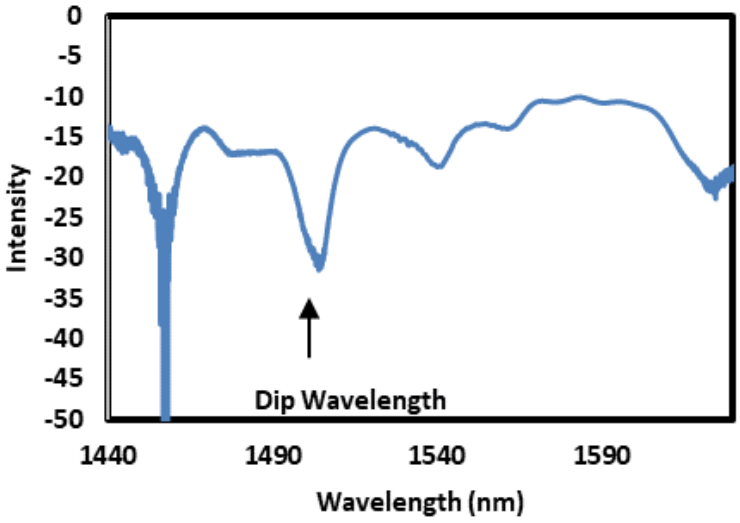

(a)

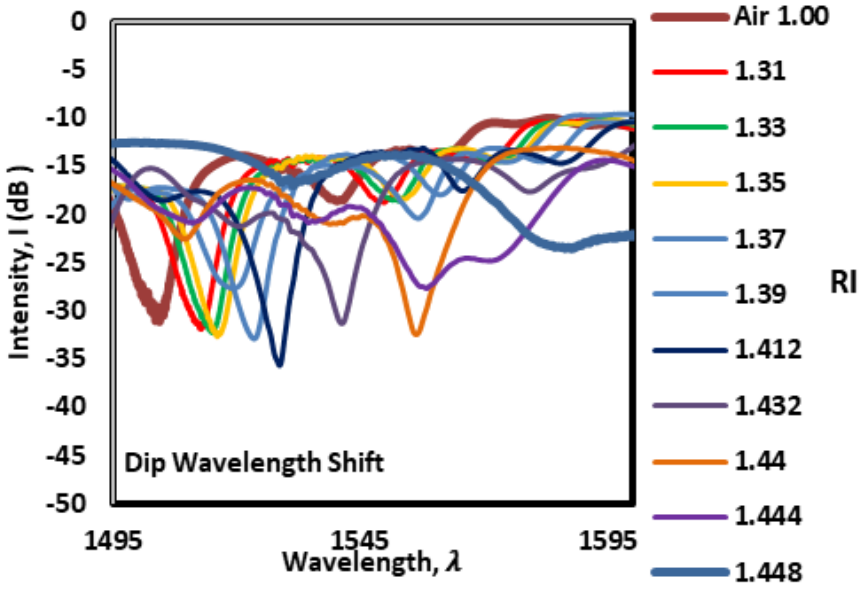

(b)

Fig. 7. Sensing spectrum from OSA (a) Transmission loss spectrum in air and (b) transmission loss with different analyte RI

The sensor's sensitivity was determined by analyzing the shifting of the dip wavelength shift on the analyte RI from 1.310 RIU to 1.448 RIU as shown in Figure 8(a). The results showed that the wavelength shift increases as the analyte RI increases, but the shift increases significantly after 1.412RIU, making it difficult to calculate the sensor's sensitivity. To obtain the sensitivity of the trench-NCF in a linear fitting, the analyte RI range is divided into two. The two subranges can be defined as Range I of 1.310–1.412 RIU and Range II of 1.412–1.448 RIU. The boundary at 1.412 RIU in the subranges is selected because from 1.412 RIU onwards the shifting of the dip wavelength started to increase compared to the earlier range. By using the least-square method as shown in Eq. (2)[3], the linear line is plotted to describe the sensor performance. The sensitivity of the sensor is represented by the gradient of the linear line as shown in Figure 8(b) and Figure 8(c).

$$\text{Gradient(Sensitivity)} = \frac{n\sum XY - \sum X \sum Y}{n\sum X^2 - (\sum X)^2} \quad (2)$$

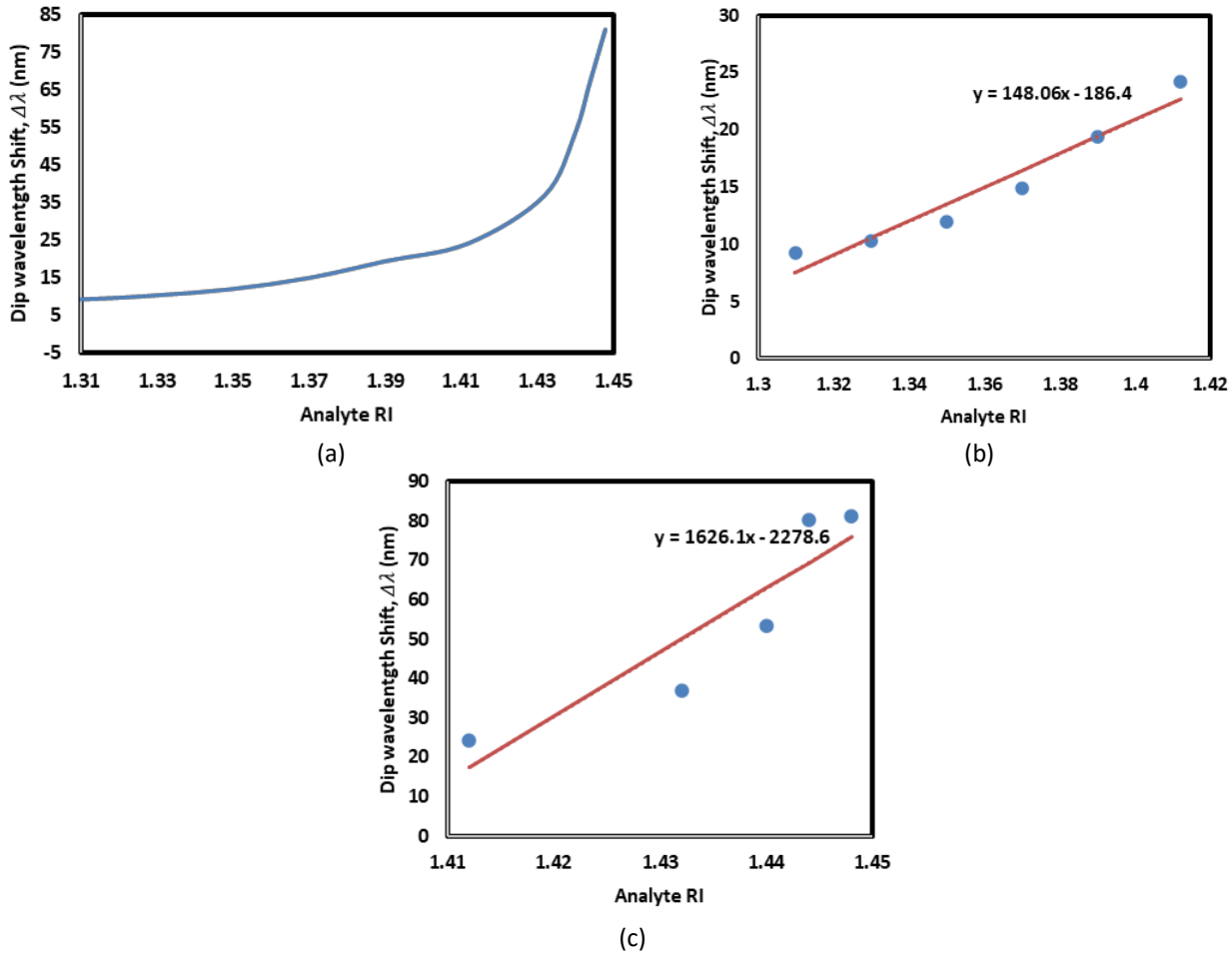

Fig. 8. Dip wavelength shift (a) full range (b) Range I and (c) Range II

4. Conclusion

In conclusion, both the objectives are achieved throughout the project. The trench-NCF was successfully simulated using COMSOL to determine the characteristics of the sensor. From the evanescent wave, it can be concluded that the electric field of the transmitted light from the light source is concentrated at the center of the trench-NCF sensor. Furthermore, the fabrication process of the trench-NCF was successfully implemented. The characterization of the sensing spectrum graph

showed that the dip wavelength is present and can be used to determine the sensor sensitivity. The dip wavelength increased when the analyte RI increased. The graph plotted in Figure 8(a) shows the nonlinearity properties and thus the sensitivity is evaluated with linear fitting by splitting the range into two from 1.310 RIU to 1.412 RIU and 1.412 RIU to 1.448 RIU respectively. The sensitivity achieved was 148.06nm/RIU and 1626.1nm/RIU respectively. The sensitivity of the trench-NCF obtained is also comparable with other refractive index sensors such as tapered fiber sensor, intensity or amplitude modulation sensor, Long Period Grating, Etched Fiber Bragg Grating and Fabry Perot interferometer. The data analyzed throughout the experiment is useful for future works and several improvements can be made such as increasing the number of samples being used to optimize the sensor performance.

References

[1] Udd, E. (1995, Aug). An Overview of Fiberoptic Sensors. Review of Scientific Instruments, 66(8), 4015-4030. https://doi.org/10.1063/1.1145411

[2] Rohizad, Siti Nur Aizatti, Suzairi Daud, Esmafatinsyafiqa Multar, Nurul Shuhada Tan Halid, and Ahmad Fakhrurrazi Ahmad Noorden. "Fibre Bragg Grating and No-Core Fibre in Variation of SRI." In *Journal of Physics: Conference Series*, vol. 1484, no. 1, p. 012008. IOP Publishing, 2020. https://doi.org/10.1088/1742-6596/1484/1/012008

[3] Brase, C. H., & Brase, C. P. (2014). Understandable statistics. Cengage Learning.

[4] Liu, Chi, Tao Shen, Hai-Bin Wu, Yue Feng, and Jiao-Jiao Chen. "Applications of magneto-strictive, magneto-optical, magnetic fluid materials in optical fiber current sensors and optical fiber magnetic field sensors: A review." *Optical Fiber Technology* 65 (2021): 102634. https://doi.org/10.1016/j.yofte.2021.102634

[5] Chung, Deborah DL. *Functional materials: Electrical, dielectric, electromagnetic, optical and magnetic applications*. Vol. 4. World scientific, 2021. https://doi.org/10.1142/12331

[6] Pendão, Cristiano, and Ivo Silva. "Optical fiber sensors and sensing networks: overview of the main principles and applications." *Sensors* 22, no. 19 (2022): 7554. https://doi.org/10.3390/s22197554

[7] Santos, José L. "Optical sensors for industry 4.0." *IEEE Journal of Selected Topics in Quantum Electronics* 27, no. 6 (2021): 1-11. https://doi.org/10.1109/JSTQE.2021.3078126

[8] Zhao, Yong, Jian Zhao, and Qiang Zhao. "Review of no-core optical fiber sensor and applications." *Sensors and Actuators A: Physical* 313 (2020): 112160. https://doi.org/10.1016/j.sna.2020.112160

[9] CABRAL, THIAGO DESTRI. "Development of Novel Optical Sensors and Applications Based on Conventional and Specialty Optical Fibers."

[10] Wu, Qiang, Yuwei Qu, Juan Liu, Jinhui Yuan, Sheng-Peng Wan, Tao Wu, Xing-Dao He et al. "Singlemode-multimode-singlemode fiber structures for sensing applications—A review." *IEEE Sensors Journal* 21, no. 11 (2020): 12734-12751. https://doi.org/10.1109/JSEN.2020.3039912

[11] Wang, Kun, Xingchen Dong, Patrick Kienle, Maximilian Fink, Wolfgang Kurz, Michael H. Köhler, Martin Jakobi, and Alexander W. Koch. "Optical fiber sensor for temperature and strain measurement based on multimode interference and square-core fiber." *Micromachines* 12, no. 10 (2021): 1239. https://doi.org/10.3390/mi12101239

[12] Yang, Wenlei, Shuo Zhang, Tao Geng, Le Li, Guoan Li, Yijia Gong, Kai Zhang et al. "High sensitivity refractometer based on a tapered-single mode-no core-single mode fiber structure." *Sensors* 19, no. 7 (2019): 1722. https://doi.org/10.3390/s19071722

[13] Feng, Yuhui, Hongyu Li, Shuguang Li, Yundong Liu, and Xiaojian Meng. "A high-sensitivity SPR refractive index sensor based on no-core fiber with ag-cu composite films." *Sensors* 21, no. 21 (2021): 7000. https://doi.org/10.3390/s21217000

[14] Liu, Yingxuan, Xuegang Li, Ya-nan Zhang, and Yong Zhao. "Fiber-optic sensors based on Vernier effect." *Measurement* 167 (2021): 108451. https://doi.org/10.1016/j.measurement.2020.108451

[15] Zhang, Jing, Chen Wang, Yunkang Chen, Yudiao Xiang, Tianye Huang, Perry Ping Shum, and Zhichao Wu. "Fiber structures and material science in optical fiber magnetic field sensors." *Frontiers of Optoelectronics* 15, no. 1 (2022): 34. https://doi.org/10.1007/s12200-022-00037-0